

Timing Measurements and Their Implications for Four Binary Millisecond Pulsars

J. F. Bell^{1,5}, M. Bailes², R. N. Manchester³, A. G. Lyne¹, F. Camilo¹ and J. S. Sandhu⁴

¹*The University of Manchester, NRAL, Jodrell Bank, Macclesfield, Cheshire SK11 9DL, UK.*

²*Physics Department, University of Melbourne, Parkville, Victoria 3052, Australia.*

³*Australia Telescope National Facility, CSIRO, PO Box 76, Epping, NSW 2121, Australia.*

⁴*Department of Astronomy, 105-24, California Institute of Technology, Pasadena, CA 91125, USA*

⁵*E-mail: jb@jb.man.ac.uk*

10 September 2021

ABSTRACT

We present timing observations of four millisecond pulsars, using data obtained over three years at the ATNF Parkes and NRAL Jodrell Bank radio telescopes. Astrometric, spin, and binary parameters are updated, and substantially improved for three pulsars, PSRs J0613–0200, J1045–4509 and J1643–1224. We have measured the time variation of the projected semi-major axis of the PSR J0437–4715 orbit due to its proper motion, and use it to constrain the inclination of the orbit and the mass of the companion. Some evidence is found for changes in the dispersion measures of PSRs J1045–4509 and J1643–1224. Limits are placed on the existence of planetary mass companions, ruling out companions with masses and orbits similar to the terrestrial planets of the solar system for eight pulsars.

Key words: Pulsars: general — pulsars: individual (PSR J0437–4715, PSR J0613–0200, PSR J1045–4509, PSR J1643–1224)

1 INTRODUCTION

Millisecond pulsars (MSPs) can be used for a variety of astrophysical applications and tests of physics. They are sensitive probes of the interstellar medium (Backer et al. 1993). They provide information about the evolution of binary systems and white dwarfs (Bhattacharya & van den Heuvel 1991), and have unsurpassed sensitivity when used to search for planetary mass bodies (Wolszczan 1994). As excellent clocks, they challenge the stability of terrestrial time standards in the best cases (Taylor 1991), place limits upon the energy density of cosmological gravitational waves (Romani & Taylor 1983; Kaspi, Taylor & Ryba 1994), and are used in testing theories of relativistic gravity (Taylor et al. 1992).

Millisecond pulsars are generally weak radio sources, and their short periods make them difficult to discover. Over the last five years several surveys have increased from four to 35, the number of millisecond pulsars known in the Galactic disk (Camilo 1996), more than half of these new discoveries resulting from the Parkes southern sky survey (Manchester et al. 1996; A. G. Lyne et al. in prep.).

In this paper we report on the timing results obtained from observations of four millisecond pulsars with data spans of over 1000 d. PSRs J0437–4715, J0613–0200,

J1045–4509 and J1643–1224 were discovered during the Parkes survey for millisecond pulsars and, with the exception of PSR J0437–4715 (Bell et al. 1995), have had only initial timing parameters reported, based on a data span of approximately one year (Bailes et al. 1994; Lorimer et al. 1995). The observations and timing analysis are described in Section 2 while the timing residuals, pulsar parameters, and pulse profiles are presented in Section 3. Observations of the time variation of the projected semi-major axis of the orbit of PSR J0437–4715 is reported in Section 4. In Section 5 we summarise all measurements of orbital eccentricities for binary pulsars while, in Section 6 we use Lomb-Scargle spectra to assess the timing residuals for evidence of planetary mass companions.

2 OBSERVATIONS AND TIMING ANALYSIS

From the time of their discovery until 1996 March, at intervals averaging about three weeks, pulse arrival times for the four MSPs were obtained using the ATNF Parkes radio telescope with cryogenic receivers at centre frequencies of 436, 660, 1520, 1940 and 2320 MHz. To date, only relatively small datasets have been obtained at 660, 1940

and 2320 MHz. Orthogonal linear polarizations were observed using a $2 \times 256 \times 0.125$ -MHz filter bank at 436 and 660 MHz while both hands of circular polarization were observed with a $2 \times 64 \times 5.0$ MHz filter bank at 1520, 1940 and 2320 MHz. After detection, the signals from the two polarizations were added, one-bit digitised at appropriate sampling intervals (0.3 ms at 436 and 660 MHz, 0.1 ms at 1520, 1940 and 2320 MHz, 0.08 ms for PSR J0437–4715) and written to magnetic tape. Off-line, the data were folded at the topocentric pulsar period to produce mean pulse profiles for each frequency channel, typically with integration times of 90–180 s. These profiles were then transformed to the Fourier domain, phase-shifted appropriately to compensate for dispersive delays across each observing band, transformed back to the time domain and summed to form a final mean profile at each frequency.

Pulse arrival times for two of the pulsars, J0613–0200 and J1643–1224, have also been obtained using the 76-m Lovell telescope at Jodrell Bank with cryogenic receivers at 408, 606, and 1404 MHz. Both hands of circular polarization were observed using a $2 \times 64 \times 0.125$ -MHz filter bank at 408 and 606 MHz and a $2 \times 32 \times 1.0$ -MHz filter bank at 1404 MHz. After detection, the signals from the two polarizations were added, filtered, digitised at appropriate sampling intervals, dedispersed in hardware before being folded on-line, and written to disk.

For both data sets, a standard pulse template was fitted to the observed profiles at each frequency to determine the pulse times-of-arrival (TOAs). The TOAs, weighted by their individual uncertainties determined in the fitting process, were analysed with the **TEMPO** software package (Taylor & Weisberg 1989), using the DE200 ephemeris of the Jet Propulsion Laboratory (Standish 1982) and the Blandford & Teukolsky (1976) timing model for binary pulsars. Using the measured TOAs and an initial set of parameters describing the pulsar system, **TEMPO** minimizes the sum of weighted squared *timing residuals*, the difference between observed and computed TOAs, yielding a set of improved pulsar parameters and post-fit timing residuals. The dispersion measures were determined by measuring the delays between the arrival times obtained at Parkes at two frequencies. We also fitted offsets between all other sets of data for each pulsar, to account for the different pulse shapes for each observing system and at different frequencies.

3 TIMING RESIDUALS, PULSAR PARAMETERS, AND PULSE PROFILES

The parameters obtained from fits to the data for each pulsar are shown in Table 1. The uncertainties quoted for these parameters are twice the formal values reported by **TEMPO**. All parameters shown in Table 1 were included in a global fit, except for \dot{P} , which was fitted for separately. The dispersion measure variation of PSR J1045–4509 was also obtained from a separate fit. For PSR J0437–4715, only 1520 to 2320-MHz data were included in the global fit due to the much larger TOA uncertainties at lower frequencies arising from the greater dispersion smearing and scintillation. In the case of PSR J1045–4509, only the 1520-MHz data were included in the global fit due to the nonmonotonic dispersion measure variation with time. For the other two pulsars all

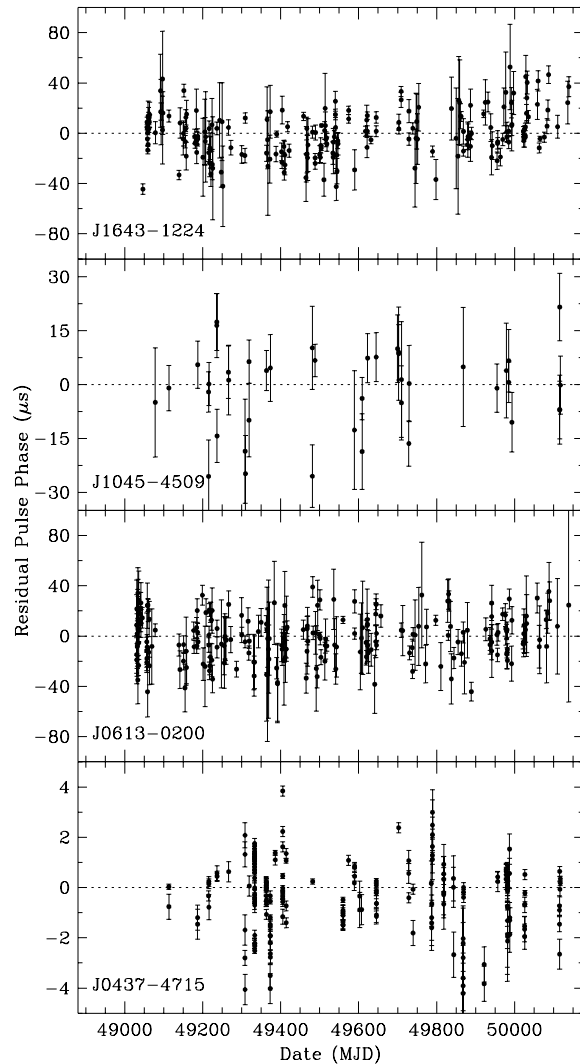


Figure 1. Post-fit timing residuals for four MSPs plotted against MJD.

available data were used. Post-fit timing residuals are shown for the four MSPs as a function of time in Fig. 1. All radio frequencies are plotted with the same symbol since there are no frequency-dependent trends in the residuals.

For PSRs J0613–0200, J1045–4509 and J1643–1224 the newly obtained celestial coordinates and binary parameters, in particular the eccentricities, are considerably improved over previously published values and are discussed in more detail in Section 5. The uncertainties in the proper motion for PSR J0437–4715 are improved by a factor of 10 while useful limits are obtained on the proper motions of the other three pulsars. The velocities shown in Table 1 were obtained using distances calculated with the Taylor & Cordes (1993) free-electron-distribution model. For PSR J0437–4715, the upper limit on the parallax of 6 mas constrains the distance to this pulsar to be greater than 166 pc (1σ), 90 pc (2σ), compared to the dispersion measure

distance of 140 pc with a 30 per cent uncertainty. Assuming that the intrinsic period derivative is zero, so that the measured period derivative is entirely due to the time-varying Doppler effect caused by the proper motion (Shklovskii 1970; Camilo, Thorsett & Kulkarni 1994), gives an upper limit on the distance of 208 pc. The upper limits on \dot{P} for the four pulsars provide no evidence for timing noise detectable with the current level of timing precision and data spans.

In some cases, deviations of the post-fit timing residuals from zero are somewhat larger than would be expected from the independently estimated TOA uncertainties. We believe that the TOA uncertainties are slightly underestimated, and we account for this in the final fitting procedure by multiplying the nominal TOA uncertainties by a small factor (typically approximately two) so as to produce a reduced χ^2 for the fit of unity. The original uncertainties are shown in the figures.

In the case of PSR J0437–4715 these deviations are very large (Fig. 1), and we believe they have a systematic origin. From one observation of this pulsar to another the ratio of the main peak intensity to that of its outlying components appears to vary by up to 20 per cent, while the ratio of the component immediately following the main peak to the underlying emission varies by factors as large as two. We do not know the exact cause of these variations, but suspect that the observed changing pulse shapes may be caused by a relative gain variation in the two polarization channels and the high degree of polarization of the emission observed across the profile (Manchester & Johnston 1995). To obtain the best set of profiles for timing, the profiles for different days were aligned and summed using the best available ephemeris. Each profile was then normalised and subtracted from the sum. The resulting difference profiles were used to select a sample of profiles most similar in shape to the mean profile, and were subsequently used to obtain the timing solution presented. In making this selection, some time-span has been sacrificed but the timing accuracy has been significantly improved. Nevertheless, the timing precision obtainable for PSR J0437–4715 with these data is not yet sufficient to measure parameters such as parallax, or the apparent orbital period derivative caused by the large proper motion of the pulsar (Bell & Bailes 1996).

Integrated pulse profiles for each of the pulsars are shown in Fig. 2 at four frequencies. In all cases the intrinsic pulse widths are narrower than the instrumental resolution. At 660 MHz the resolution for all four pulsars is determined by the sampling interval, as is the resolution of the PSR J0437–4715 profiles at 436 and 1520 MHz. The resolution of the remaining profiles is dominated by dispersion smearing across individual channels. Hence, for these pulsars, the profiles observed at 1520 and 436 MHz are broader than the corresponding profiles at 2320 and 660 MHz. The asymmetry and tail of the PSR J1643–1224 profile at 436 MHz suggests some evidence for scattering along the line of sight to this pulsar. The scattering time-scale τ_s (Taylor, Manchester & Lyne 1993) as measured from the pulse profile in Fig. 2, is approximately 240 μ s at 436 MHz. After scaling to 1 GHz by $\nu^{-4.4}$ (Cordes, Weisberg & Boriakoff 1985), $\tau_{s,1\text{GHz}} = 6 \mu$ s and is comparable to the scattering time-scales of other pulsars with similar dispersion measures (Taylor, Manchester & Lyne 1993). It is

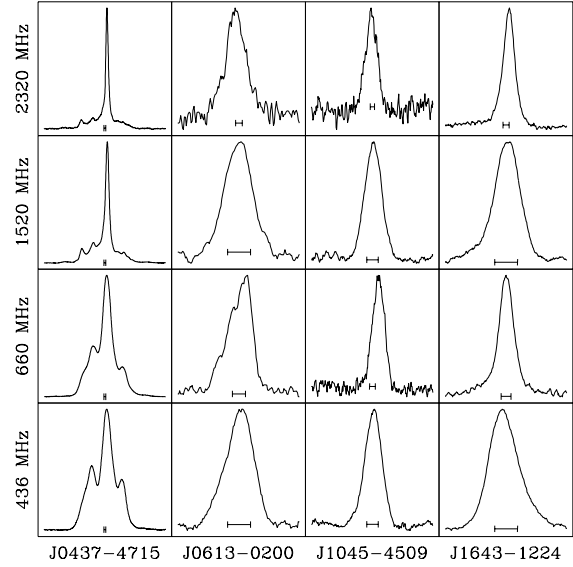


Figure 2. Integrated pulse profile for each pulsar at four frequencies. In each case the full period is shown and the instrumental resolution is indicated by a horizontal bar.

however, somewhat higher than the 0.7 μ s predicted by the Taylor & Cordes (1993) model.

We have observed dispersion measure variations for PSRs J1045–4509 and J1643–1224 and obtained an upper limit on the variations for PSR J0613–0200 as shown in Table 1. In the case of PSR J1045–4509, DM was fitted over the first half of the data span only, where the variation is monotonic. To illustrate the variations for PSRs J1643–1224 and J1045–4509, the best fit to the Parkes 1520-MHz data was made. For PSR J1045–4509 the DM was fitted around MJD 49500 and for PSR J1643–1224 the DM was fitted around MJD 49100. The residuals for the 436-MHz Parkes data were then calculated and plotted with the 1520-MHz data in Fig. 3.

Backer et al. (1993) summarized observations of dispersion measure variations for 13 pulsars and found that the rate of change of dispersion measure, $\Delta DM \propto \sqrt{DM}$. This is somewhat flatter than the linear dependence observed for diffractive scattering (Cordes, Pidwerbetzky & Lovelace 1986). Dispersion measure variations sample electron-density fluctuations on length scales of 10^{13} – 10^{15} cm, which are 10^4 times larger than the scale of the fluctuations which lead to diffractive scattering. This difference in variation with dispersion measure suggests that these two effects may occur at different locations along the line of sight, or have different driving mechanisms. Our results are in general agreement with $\Delta DM \propto \sqrt{DM}$ and therefore the conclusions drawn by Backer et al., although the scatter of the data about this relation is large.

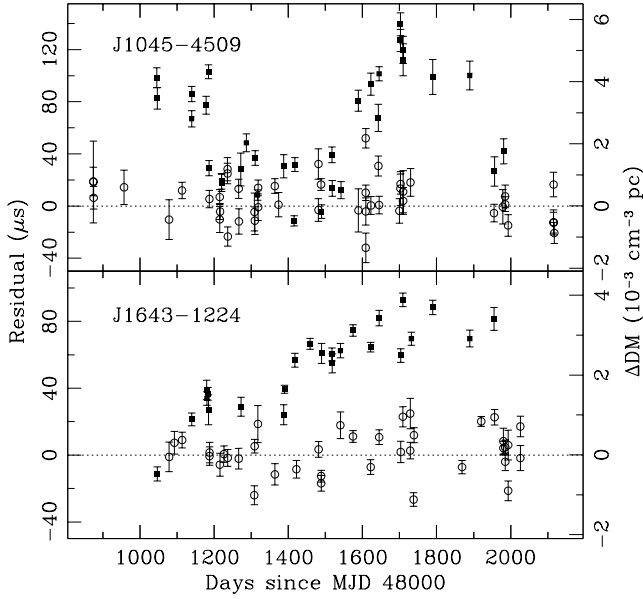


Figure 3. Dispersion measure variations in two pulsars. Timing residuals from Parkes data at 436 MHz (filled squares) and 1520 MHz (circles), relative to a timing model fitted to the latter. Note the systematic variations in the difference between the two frequencies.

4 SECULAR VARIATION OF ORBITAL INCLINATION

It has been recently noted that the proper motion of a pulsar can lead to a secular variation of the projected semi-major axis of the pulsar’s orbit, $a_p \sin i$, as the orbital inclination i changes (Arzoumanian et al. 1996; Kopeikin 1996; Sandhu et al. 1997). The contribution to the time derivative of the projected semi-major axis is

$$\dot{x} = 1.54 \times 10^{-16} x \cot i (-\mu_\alpha \sin \Omega + \mu_\delta \cos \Omega), \quad (1)$$

where $x = a_p \sin i / c$ is the projected orbital light travel time in seconds, Ω is the longitude of the ascending node of the orbit, and μ_α and μ_δ are the proper motions in right ascension and declination, in mas yr^{-1} (Kopeikin 1996). Both the proper motions can be measured, while Ω cannot, so that a measurement of \dot{x} allows a constraint to be placed on i and hence the mass of the companion and on many aspects of the evolution of these systems.

The types of system for which this method works well are those that have wide, small inclination (i.e. face-on) orbits, that are relatively nearby. It is therefore complementary to the measurement of the “Shapiro delay”, which produces measurable effects for high-inclination (edge-on) systems in tight orbits. For millisecond pulsars with white-dwarf companions, the orbit needs to be very close to edge on for the Shapiro delay to be measurable. For intermediate inclination angles, where some evidence of Shapiro delay is visible but where the covariance between the fitted companion mass and inclination angle is great (e.g. in the PSR J1713+0747 system, with $i \sim 70^\circ$, Camilo, Foster, & Wolszczan 1994), measurement of \dot{x} may be possible and should provide an additional constraint on the system.

From the observations of PSR J0437–4715, the measured value of $\dot{x} = (7.4 \pm 1.4) \times 10^{-14}$ implies that $\dot{x} > 6 \times 10^{-14}$. Due to the non-Gaussian distribution of the timing residuals, we used bootstrap resampling (Press et al. 1992) to derive the uncertainties on all parameters in Table 1, including \dot{x} . For most parameters, this yields similar uncertainties to those calculated in the standard way from a least-squares fit. However, for PSR J0437–4715, the uncertainties on \dot{x} and x are eight times larger using bootstrap resampling. We therefore take the more conservative bootstrap uncertainties as the 68 per cent confidence level. The maximum contribution from the proper motion occurs when the proper motion is aligned with the semi-major axis of the orbit projected onto the plane of the sky. This yields a limit of $\cot i > 6.5 \times 10^{15} \dot{x} / (x\mu) = 0.83$, giving an upper limit of $i < 50^\circ$. Consequently, the companion mass is constrained to be greater than $0.19 M_\odot$, for an assumed pulsar mass of $1.4 M_\odot$, considerably more than the *a priori* minimum possible value of $0.14 M_\odot$.

One may easily show that the measured \dot{x} cannot be due to a genuine shrinking of the orbit. Since $\dot{x} = \dot{a}_p / c \sin i + a_p / c \cos i \, di/dt$, one must ensure that $\dot{a}_p \sin i \ll a_p \cos i \, di/dt$. This can be checked by obtaining an observational limit on \dot{P}_b and differentiating Kepler’s third law with respect to time, which gives \dot{a}_p as a function of \dot{P}_b . Inserting the observed limit for PSR J0437–4715 of $\dot{P}_b < 2.2 \times 10^{-11}$ shows that $\dot{x} < 3.1 \times 10^{-15}$ which is indeed much smaller than the measured value of \dot{x} , and hence shows that $\dot{x} \simeq a_p / c \cos i \, di/dt$. The negligible value of \dot{a}_p is exactly as expected since orbital evolution due to gravitational radiation or tidal effects leads to values of \dot{a}_p many orders of magnitude smaller than observed for \dot{x} .

5 ORBITAL ECCENTRICITIES

The timing observations presented here, vastly improve the accuracy of the eccentricity measurements, particularly for PSRs J0613–0200 and J1643–1224. In this section, we collate all such measurements of, and upper limits on, eccentricities of binary pulsar orbits and compare them with theoretical predictions.

The convective fluctuation-dissipation theory of Phinney (1992) predicts a strong correlation between the orbital eccentricities and orbital periods of binary pulsars that have been recycled by stable mass-transfer from a Roche-lobe-filling, low-mass red giant. The measured eccentricities together with upper limits are shown for all Galactic binary pulsars in Fig. 4. All measurements (circles) and upper limits (squares) for objects with appropriate evolutionary histories are in excellent agreement with the model. As shown by the dashed lines, the trend of the upper limits for those objects with short orbital periods is merely a reflection of the timing precision attainable.

Neutron stars in highly eccentric orbits have provided some remarkable tests of general relativity and other theories of gravity (Taylor et al. 1992). There are also interesting and useful tests than can be done using neutron stars in very circular orbits: tests of the strong equivalence principle (Damour & Schäfer 1991), of local Lorentz invariance (Damour & Esposito-Farèse 1992) and of conservation laws (Bell & Damour 1996). These latter two tests depend lin-

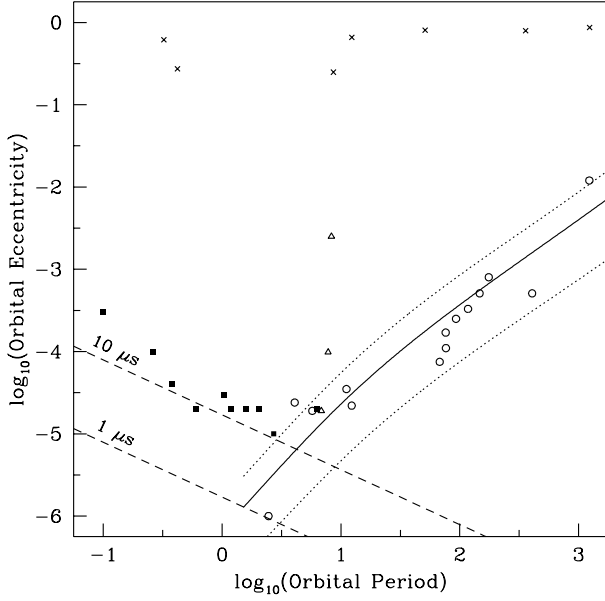


Figure 4. Orbital eccentricities from Table 2 of Camilo (1996) and this paper. Solid line — the predicted median eccentricity for pulsars recycled by stable mass transfer from a Roche-lobe-filling, low-mass red giant. Dotted lines — 95 per cent of the measured eccentricities for recycled pulsars are expected to lie within these (Phinney 1992; Phinney & Kulkarni 1994). Circles — low-mass binary pulsars. Squares — upper limits on measured eccentricities. Crosses — high-mass binary pulsars. Triangles — intermediate-mass binary pulsars. Dashed lines — approximate limits obtainable on eccentricities for timing residuals of $10 \mu\text{s}$ and $1 \mu\text{s}$.

early on the orbital eccentricity of a sample of binary millisecond pulsars.

The orbit with the lowest eccentricity in Fig. 4, and in fact the known universe, is PSR J2317+1439 (Camilo, Nice & Taylor 1996). This has been used to obtain a very tight limit on the local Lorentz invariance of gravity (Bell, Camilo & Damour 1996). However, due to an unfavourable orientation of its position and proper motion with respect to the dipolar structure of the cosmic microwave background, the limit is not as tight as it might otherwise be. The predicted eccentricities for some millisecond pulsars (e.g. PSR J0613–0200) are somewhat lower than that of PSR J2317+1439, suggesting that these systems may ultimately provide more stringent tests of local Lorentz invariance, and may also allow the tests of the strong equivalence principle and conservation laws to be improved. However, as Fig. 4 shows, this will require timing precisions of about $1 \mu\text{s}$, which will be very difficult to achieve. Nevertheless, any improvement on timing precision for the pulsars with only upper limits on eccentricity will provide further tests of the fluctuation-dissipation theory.

6 LIMITS ON PLANETARY MASS COMPANIONS

The discovery of planetary mass companions to a millisecond pulsar (Wolszczan & Frail 1992) was unexpected. Their existence has been confirmed by the detection of three-body

perturbations in the timing residuals (Wolszczan 1994). Naturally, such a discovery stimulates interest in finding other MSPs with planetary mass companions. In this Section, we place limits on the existence of any planetary mass companions to the pulsar discussed in this paper using Lomb-Scargle spectra. While these pulsars have stellar-mass companions and may be less likely to have planetary companions, we apply the same technique to four single pulsars in another paper (M. Bailes et al. in prep.).

From the residuals shown in Fig. 1 there appears to be no evidence for modulations that could be attributed to planetary mass companions. The mass function for a pulsar binary is given by

$$f = \frac{(m_c \sin i)^3}{(m_p + m_c)^2} = \frac{4\pi^2 (a_p \sin i)^3}{GP_b^2} \quad (2)$$

where i is the inclination angle of the orbit, a_p is the semi-major axis of the pulsar's orbit, P_b is the orbital period, G is the gravitational constant and m_p and m_c are the pulsar and companions masses. Assuming circular orbits and $m_c \ll m_p$, rearranging equation 2 suggests upper limits on the mass of undetected companions of

$$m_c \sin i = a_p \sin i \left(\frac{4\pi^2 m_p^2}{GP_b^2} \right)^{1/3} \quad (3)$$

$$\leq 0.0143 M_\oplus \Delta T_a \left(\frac{P_b}{1 \text{ day}} \right)^{-2/3} \quad (4)$$

where ΔT_a is the timing signal (peak-peak delay) due to the light travel time across the pulsar's orbit and M_\oplus is the mass of the Earth. If no modulation is seen in the residuals, a limit on ΔT_a of an unseen companion can be obtained from the variance of the residuals, allowing a limit to be placed on $m_c \sin i$. For long orbital periods the sensitivity drops as P_b^3 due to the strong covariance between the orbital period of a planet and the period derivative of the pulsar (Thorsett & Phillips 1992).

The above limits should be considered as qualitative. Quantitative limits on the presence of modulations can be obtained through a number of approaches: fast Fourier transforms (FFTs), fold and average, fitting of orbits (Thorsett & Phillips 1992), and Lomb-Scargle spectra (Lomb 1976; Scargle 1982; Press et al. 1992). Each of these methods has various advantages and disadvantages which are now briefly discussed. Fold and averaging, and fitting orbits to residuals are computationally expensive, provide poor detectability and sensitivity and do not offer a statistical assessment of the significance of any signals detected. FFTs overcome all of these difficulties, but suffer from aliasing and poor sensitivity to long orbits resulting from the need to fill in gaps in the unevenly sampled data.

The Lomb-Scargle periodogram overcomes these difficulties and is similar in speed to the FFT when one accounts for the additional data points required to provide the even sampling for the FFT. It also allows one to search for frequencies up to several times the mean Nyquist frequency. However, both the Lomb-Scargle periodogram and the FFT fail to take account of the covariance with other effects such as the Earth's orbit, which causes a loss of sensitivity for periods around one year (Thorsett & Phillips 1992). A distinct advantage of the spectral methods is that they do allow a formal assessment of the statistical significance of spectral

features, taking account of the number of frequencies that were searched. An ideal analysis therefore might consist of a Lomb-Scargle periodogram, combined with a small selection of fitted orbits to account for the above covariance problems.

In this paper, examples of Lomb-Scargle spectra of the timing residuals for eight pulsars are given in Figs. 5 and 6. Four of the pulsars are those discussed in this paper and the remaining four are discussed in Camilo et al. (in prep.). The spectra as a function of frequency were converted to a function of period, while the timing signal was obtained using $\Delta T_a = 2 \times 2(P_a/N_0)^{0.5}$, where P_a is the spectral power and N_0 is the number of independent data points (Scargle 1982). Equation 4 was then used to convert to units of $m_e \sin i$. To account for the covariance with the period derivative of the pulsar, the limits were multiplied by P_b^3 for periods greater than one year.

To test the sensitivity of the method, the eccentricity of PSR J1643–1224 was adjusted by 0.24 per cent which is precisely three times the uncertainty in the measured value shown in Table 1. The resulting Lomb-Scargle spectrum in the lower panel of Fig. 5 shows a highly significant detection. The probability that this signal is due to random noise is 1.5×10^{-5} . As another test of this method, the Jodrell Bank timing residuals for PSR B1257+12 were analysed in the same manner. After fitting for a slow-down model of the pulsar, the spectrum of the residuals (bottom panel of Fig. 6) shows highly significant signals at the periods of the planets. The probability that these spikes are due to random noise is 2.8×10^{-8} . It is important to note that the side lobes resulting from the uneven sampling of the data are very strong at all periods. For example, in the B1257+12 spectrum, the rms is totally dominated by the side lobes, while the true noise level for this pulsar is similar to that of the other pulsars shown in Figs. 5 and 6. This slightly increased rms may also be seen by comparing the spectrum for PSR J1643–1224 with the fake spectrum below it in Fig. 5.

There are no spectral features that give any hint that a detectable periodic signal is present in the residuals of any of the eight MSPs considered. Probabilities of 0.1 and 0.999, that the signals are due to random noise are shown by the smooth curves in the figures, indicating that to a very high level of significance, the timing residuals are purely random. For the eight MSPs discussed here, companions with masses and orbits similar to Venus, Earth and the two largest planets around PSR B1257+12 are ruled out. For those MSPs with more precise timing results, such as PSR J0437–4715, the existence of companions with masses and orbits similar to Mercury and Mars are also ruled out.

ACKNOWLEDGMENTS

The authors are grateful to the referee Alex Wolszczan for helpful comments and suggestions.

REFERENCES

Arzoumanian Z., Joshi K., Rasio F., Thorsett S. E., 1996, in Johnston S., Walker M. A., Bailes M., eds, Pulsars: Problems and Progress, IAU Colloquium 160. Astronomical Society of the Pacific, p. 525

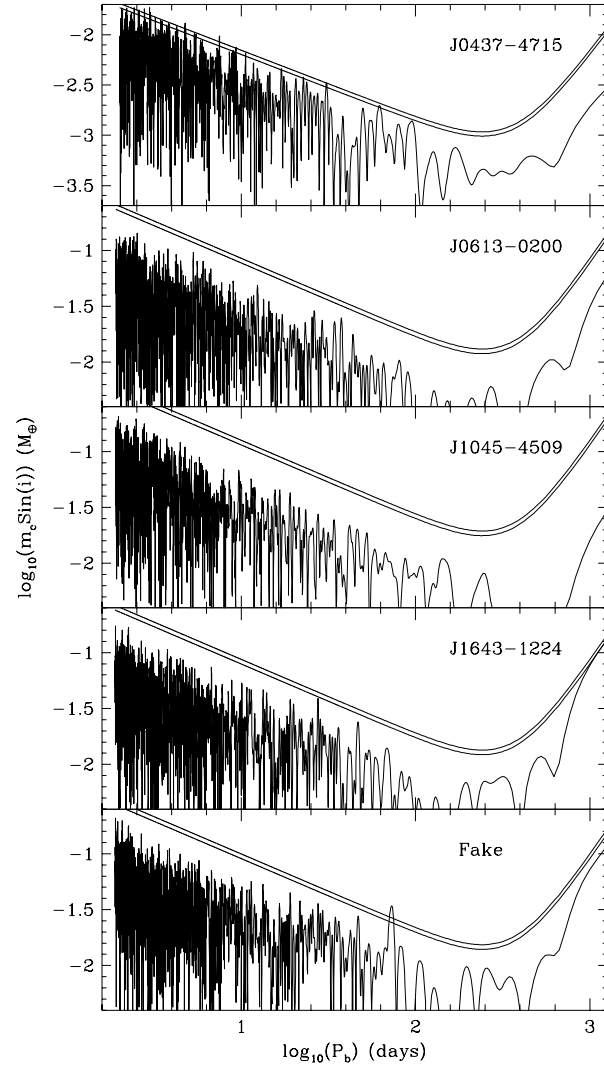


Figure 5. The top four panels show Lomb-Scargle spectra of timing residuals for pulsars in this paper. In each panel the two smooth curves indicate the 0.1 and 0.999 probabilities that a signal is due to random noise. Thus features above the line are likely to be significant signals and those below the line, noise. The lower panel shows the result of modifying the eccentricity of PSR J1643–1224 to introduce a fake sinusoidal signal at half the orbital period. A significant detection is seen at precisely this period.

Backer D. C., Hama S., Van Hook S., Foster R. S., 1993, *ApJ*, 404, 636
 Bailes M. et al., 1994, *ApJ*, 425, L41
 Bell J. F., Bailes M., 1996, *ApJ*, 456, L33
 Bell J. F., Damour T., 1996, *Classical Quantum Gravity*, In Press
 Bell J. F., Camilo F., Damour T., 1996, *ApJ*, 464, 857
 Bell J. F., Bailes M., Manchester R. N., Weisberg J. M., Lyne A. G., 1995, *ApJ*, 440, L81
 Bhattacharya D., van den Heuvel E. P. J., 1991, *Phys. Rep.*, 203, 1
 Blandford R., Teukolsky S. A., 1976, *ApJ*, 205, 580

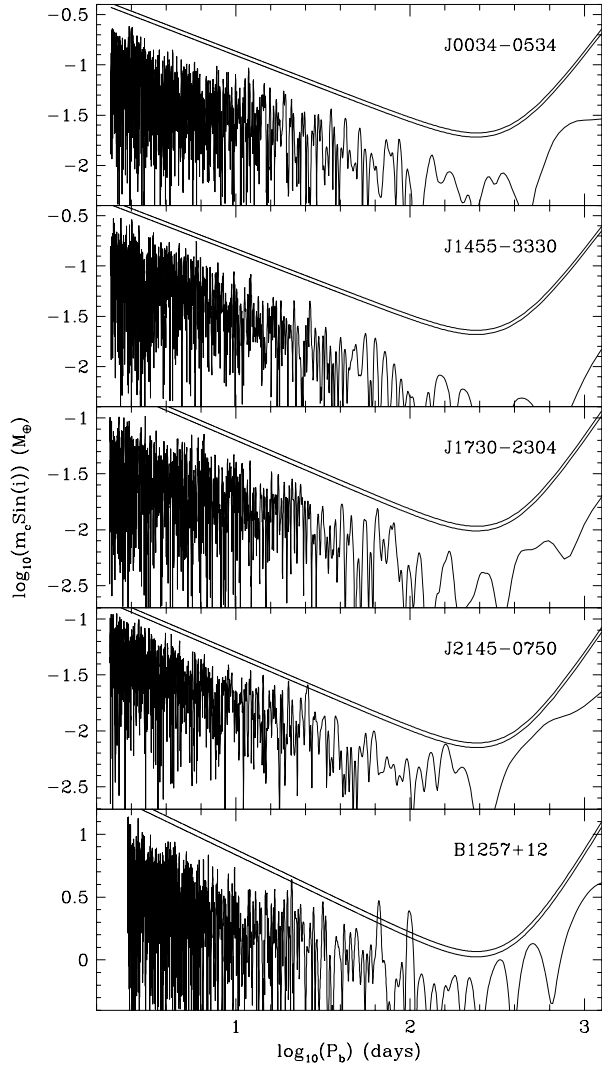


Figure 6. Lomb-Scargle spectra of timing residuals for the four pulsars discussed by Camilo et al. (1996), as for Fig. 5. In this case the lower panel shows a spectrum of the Jodrell Bank timing residuals for PSR B1257+12 which is known to have planets.

Manchester R. N., Johnston S., 1995, *ApJ*, 441, L65
 Manchester R. N. et al., 1996, *MNRAS*, 279, 1235
 Phinney E. S., Kulkarni S. R., 1994, *ARAA*, 32, 591
 Phinney E. S., 1992, *Philos. Trans. Roy. Soc. London A*, 341, 39
 Press W. H., Teukolsky S. A., Vetterling W. T., Flannery B. P.,
 1992, *Numerical Recipes: The Art of Scientific Computing*,
 2nd edition. Cambridge University Press, Cambridge
 Romani R. W., Taylor J. H., 1983, *ApJ*, 265, L35
 Sandhu J. S., Bailes M., Manchester R. N., Navarro J., Kulka-
 rni S. R., Anderson S. B., 1997, *ApJ*, submitted
 Scargle J. D., 1982, *ApJ*, 263, 835
 Shklovskii I. S., 1970, *Sov. Astron.*, 13, 562
 Standish E. M., 1982, *A&A*, 114, 297
 Taylor J. H., Cordes J. M., 1993, *ApJ*, 411, 674
 Taylor J. H., Weisberg J. M., 1989, *ApJ*, 345, 434
 Taylor J. H., 1991, *Proc. I. E. E. E.*, 79, 1054
 Taylor J. H., Manchester R. N., Lyne A. G., 1993, *ApJS*, 88, 529
 Taylor J. H., Wolszczan A., Damour T., Weisberg J. M., 1992,
Nature, 355, 132
 Thorsett S. E., Phillips J. A., 1992, *ApJ*, 387, L69
 Wolszczan A., Frail D. A., 1992, *Nature*, 355, 145
 Wolszczan A., 1994, *Science*, 264, 538

Camilo F., 1996, in Jackson N., ed, *High Sensitivity Radio As-
 tronomy*. Cambridge University Press, In Press
 Camilo F., Foster R. S., Wolszczan A., 1994, *ApJ*, 437, L39
 Camilo F., Nice D. J., Taylor J. H., 1996, *ApJ*, 461, 812
 Camilo F., Manchester R. N., Bailes M., Lyne A. G., Bell J. F.,
 1997, *ApJ*, In preparation
 Camilo F., Thorsett S. E., Kulkarni S. R., 1994, *ApJ*, 421, L15
 Cordes J. M., Pidwerbetsky A., Lovelace R. V. E., 1986, *ApJ*,
 310, 737
 Cordes J. M., Weisberg J. M., Boriakoff V., 1985, *ApJ*, 288, 221
 Damour T., Esposito-Farèse G., 1992, *Phys. Rev. D*, 46, 4128
 Damour T., Schäfer G., 1991, *Phys. Rev. Lett.*, 66, 2549
 Kaspi V. M., Taylor J. H., Ryba M., 1994, *ApJ*, 428, 713
 Kopeikin S. M., 1996, *ApJ*, 467, L93
 Lomb N. R., 1976, *Ap. Space Sci.*, 39, 447
 Lorimer D. R. et al., 1995, *ApJ*, 439, 933

Table 1. Parameters of millisecond pulsars J0437–4715, J0613–0200, J1045–4509, and J1643–1224. Figures in parentheses represent 1σ uncertainties in the last significant digits quoted. Some values of T_0 and ω are given to greater precision than the available accuracy to help observers.

	PSR J0437–4715	PSR J0613–0200	PSR J1045–4509	PSR J1643–1224
α (J2000)	04 ^h 37 ^m 15 ^s .73501(2)	06 ^h 13 ^m 43 ^s .97317(14)	10 ^h 45 ^m 50 ^s .1940(3)	16 ^h 43 ^m 38 ^s .1548(2)
δ (J2000)	−47°15′08″.1527(2)	−02°00′47″.072(6)	−45°09′54″.204(2)	−12°24′58″.740(14)
μ_α (mas yr ^{−1})	121.3(2)	1.5(30)	−7(3)	7(3)
μ_δ (mas yr ^{−1})	−70.4(3)	−4(6)	8(2)	7(17)
π (mas)	1(5)
P (ms)	5.75745182325672(13)	3.0618440360787(6)	7.4742241050635(10)	4.6216414453446(9)
\dot{P}	$5.7296(8) \times 10^{-20}$	$9.57(4) \times 10^{-21}$	$1.740(8) \times 10^{-20}$	$1.840(6) \times 10^{-20}$
$ \dot{P} $ (s ^{−1})	$< 1.4 \times 10^{-30}$	$< 5 \times 10^{-30}$	$< 14 \times 10^{-30}$	$< 8 \times 10^{-30}$
Epoch (MJD)	49615.0	49512.0	49597.0	49524.0
DM (cm ^{−3} pc)	2.649(4)	38.7911(5)	58.1833(18)	62.4133(4)
$\dot{D}M$ (cm ^{−3} pc yr ^{−1})	0.0003(4)	−0.0049(13)	0.0010(5)
P_b (d)	5.741042355(3)	1.198512557(3)	4.083529188(17)	147.017395(2)
x (s)	3.3666820(4)	1.091445(5)	3.015128(4)	25.072613(4)
\dot{x}	$7.4(14) \times 10^{-14}$	$< 20 \times 10^{-14}$	$9(14) \times 10^{-14}$	$< 16 \times 10^{-14}$
e	$1.86(3) \times 10^{-5}$	$7(10) \times 10^{-6}$	$2.4(3) \times 10^{-5}$	$5.057(4) \times 10^{-4}$
ω	$2^\circ 18'11'' \pm 0.72$	$43^\circ 04'40'' \pm 36.5$	$226^\circ 07'87.15'' \pm 10$	$321^\circ 8'57.8'' \pm 0.04$
T_0 (MJD)	49615.852918±0.01	49512.409269±0.2	49598.199375±0.1	49577.972054±0.015
\dot{P}_b	$< 2.2 \times 10^{-11}$
μ (mas yr ^{−1})	140.2(3)	4(6)	11(3)	10(13)
d (kpc)	0.14	2.2	3.2	>4.9
v (km s ^{−1})	93(30)	40(60)	168(45)	...
RMS residual (μ s)	1.1	15	10	14
Frequencies in fit (MHz)	1520, 1940 & 2320	400, 600 & 1400	1400	400, 600 & 1400
Data span (MJD)	49113–50117	49030–50138	49078–50117	49046–50139